JNTM JOURNAL of NEW TECHNOLOGY and MATERIALS

Journal of New Technology and Materials

Vol. 14, No. 1 (2024), 21–32

RESEARCH ARTICLE

Lattice-Conditioned Arrhenius Residual Learning for Phase-Resolved Hydrogen Transport in Titanium Hydrides

T. Layne[1,*], W. Kim[2] and J. E. Greene[2]

[1]Department of Materials Science and Engineering, Yonsei University, 50 Yonsei-ro, Seodaemun-gu, Seoul 03722, Republic of Korea. [2]Materials Research Laboratory and Materials Science Department, University of Illinois, 104 South Goodwin, Urbana, Illinois 61801

*Correspondence: layne29@@yonsei.ac.kr
Received date: December 11, 2023; Accepted date: March 18, 2024

Abstract

Modeling hydrogen mobility in titanium hydrides on the basis of a single diffusivity is impossible due to the different connectivity, activation energy, and heat capacity of the face-centered cubic (FCC), body-centered cubic (BCC), and hexagonal close-packed (HCP) titanium–hydrogen compounds. This paper presents a new lattice-conditioned Arrhenius residual learning algorithm (LC-ARL) to convert predictions of the diffusion process based on lattice moment tensor potentials into the temperature dependence of the physically meaningful diffusivity value. The main problem to be solved here concerns whether a residual mapping could provide the physically meaningful ordering between Ti-H phases and which Ti-H transport phase needs further physical validation by characterizing its effective diffusivity. The developed LC-ARL algorithm includes two-dimensional evaluation of residual spaces for MTP-AL and MTP-DIRECT moment tensor potentials, determination of the phase-resolved reliability weighting factor, calculation of Arrhenius prefactor parameters using reference state diffusivities, and construction of Arrhenius diffusivity curves based on phase-resolved geometric average. The selected phase-resolved validation examples are FCC Ti648H1296, BCC Ti648H648, and dilute HCP Ti648H36. LC-ARL leads to the much lower mean absolute activation energy error (0.0084 eV) relative to MTP-AL (0.0567 eV) and MTP-DIRECT (0.0167 eV) algorithms without increasing the mean absolute logarithmic diffusivity error (identical 0.074 decade). Moreover, the temperature sweep preserves the Ti-H transport phase sequence BCC > HCP >> FCC within the 300-1000 K range. Thus, the proposed research question was positively answered concerning this particular data set – a combination of magnitude and slope errors resulted in physically meaningful Arrhenius diffusivity function. Dilute HCP titanium hydride was identified as the most appealing validation example because of non-coordinated optimization of magnitude and activation energy.

Keywords: titanium hydride, hydrogen diffusion, machine learning interatomic potential, Arrhenius modelling, moment tensor potential, residual learning, phase-aware transport

1 Introduction

Ti and its alloys are selected for aerospace structural components, biomedical implants, marine parts, equipment for chemical processing, and electrochemical devices due to low density, high specific strength, corrosion resistance, and phase transformability. Among the challenges posed by these metals is a tendency to incorporate hydrogen as a consequence of corrosion, cathodic polarization, exposure to acids, thermal treatment, welding, hydrogen service, and interaction with hydrogen-containing media. Hydrogen is absorbed and subsequently distributed in the interstitial lattice sites in titanium. It can migrate along lattice channels, react with point defects and crystal stresses, and form new phases called hydrides. In contrast to metallic Ti, the hydride phase has quite a distinct mechanical and diffusion behavior. Hence, the analysis of hydrogen behavior in Ti is not merely a matter of the equilibrium properties of the Ti–H alloy but also a transport

issue. The rate of hydrogen migration, the direction, and the kinetics of transformation can significantly influence hydride growth, local embrittlement, and service stability [2–4].

Modelling hydrogen behavior in titanium is complicated by the following facts. The word “diffusivity" does not refer to one single kinetic state. In the compact close-packed lattice structure, the motion of an interstitial atom is hindered by its connections to neighbors, local distortion, and the energy required to reach transition configurations. In a more spacious BCC-like configuration, the same element can freely migrate within an open network characterized by a low energy barrier. Moreover, an FCC titanium dihydride can be interpreted as a hydrogen-rich phase with low diffusivity and a high energy barrier. A BCC hydride is considered a phase with fast hydrogen migration and a low energy barrier. HCP titanium in dilute states contains a few hydrogen atoms per unit cell and, hence, exhibits a more complex diffusion behavior than its FCC and BCC relatives. Experimental results for hydrogen transport in titanium alloys show activation energies of 0.45 eV, 0.15 eV, and 0.92 eV in HCP, BCC, and FCC titanium dihydrides, respectively [5–7]. As can be seen, hydrogen migration in different Ti phases is characterized by quite different kinetic conditions and an averaged diffusivity cannot provide the essential kinetic detail required for predicting hydrogen evolution in Ti.

A consideration of hydride growth, morphological transitions, embrittlement, and hydrogen-assisted failure highlights the significance of accurate diffusion in each Ti phase. The traditional approach to hydrogen diffusion in metals is based on several mechanisms, including trapping, hydrogen-enhanced localized plasticity, decohesion, and stress-assisted diffusion, which are distinct but interact with each other [8–10]. The kinetics of these processes depends not only on material chemistry but also on microstructure, texture, phase ratio, hydride precipitation, and thermal annealing. The model that underestimates the mobility of a BCC-like phase will fail to describe a rapid supply of hydrogen to critical zones in Ti. On the contrary, the overestimated FCC diffusion constant will yield incorrect predictions for the sluggish growth of a hydrogen-rich hydride precipitate. In this case, the goal is not to obtain a single number, but to keep the essential role of each lattice.

The extensive body of literature devoted to hydrides reveals the significant importance of interstitial migration for hydrogen behavior in metals. Standard models of metal–hydrogen interactions focus on solubility, diffusion, trapping, and phase separation as processes that depend not only on lattice structure but also on thermodynamic conditions [11–13]. For the Ti–H alloy, the diffusion process in a dilute HCP metal, stoichiometric hydrides, and mobile hydride phases cannot be considered similar. A valid diffusion model, hence, should reflect the transport activity of each of these phases and should be characterized by high diffusivity and activation-energy fidelity. Computational approaches based on density functional theory (DFT) and *ab initio* molecular dynamics allow obtaining high-accuracy results with respect to atomic bonds, but are too expensive for large supercells and long trajectories at elevated temperatures. Therefore, classical potentials are used to simulate migration processes in a broad temperature range, but such an approach can lead to the inaccuracy for materials including a dilute HCP lattice, stoichiometric hydride phases, multiple lattice types, and high-temperature structures. The development of machine learning interatomic potentials has become necessary for accurate modelling of various materials and is based on approximating the underlying potential-energy surfaces with a lower computational cost [14–16].

Machine learning potentials are now successfully applied to all kinds of interatomic interactions including those based on neural networks [17], Gaussian approximation potentials [18], moment tensors [19], graph neural networks [**?**], and universal materials potentials [**?**]. However, their reliability highly depends on the choice of training environments that should include the configurations observed in experiments. Active-learning and uncertainty-guided training algorithms can improve the quality of a potential by selecting informative atomic arrangements and avoiding unnecessary electronic-structure computations [21–23]. Recently proposed dimensionality-reduction approaches to sampling have shown that an efficient encoding of the lattice environment leads to better results for more complex potential spaces. In particular, this methodology was applied to Ti–H moment tensor potentials [1].

However, the diffusion process is described not solely by energy barriers and atomic potentials. Hydrogen migration and transport properties in a material can be affected by interparticle distances, coordination, and lattice arrangement. Therefore, even a small error in forces, energy barriers, or geometry can result in distorted long-time behavior of hydrogen atoms. The diffusion process in Ti–H phases is particularly susceptible to inaccuracy since activation energy and diffusivity magnitude play completely different roles. The activation energy is responsible for diffusion sensitivity to temperature variation. The latter parameter determines transport at a specific temperature where reliable data are available. The Arrhenius law connects the diffusion constant and activation energy. Nevertheless, agreement in temperature sensitivity cannot be considered equal to agreement in diffusivity magnitude.

In this study, a phase-resolved Arrhenius residual learning is used to solve the problem in question. This approach implies the analysis of diffusion transport properties in each lattice type using existing information about hydrogen migration in a certain phase. Unlike training-based correction schemes, it focuses on the fusion of transport estimates using residual Arrhenius parameters without changing the potentials or interpreting existing atomistic trajectories. A lattice-dependent weighting strategy is suggested that allows obtaining a set of Arrhenius curves that reflect the true physical behavior of diffusion in each lattice.

The main research question is the following. Is it possible to use a residual learning scheme to fuse two atomistic transport estimations and preserve both the phase order of diffusivity magnitude and the uncertainty of each phase? In

this study, we assume that each phase is characterized by different kinetic conditions. This implies that the slope of an Arrhenius curve is significant for FCC titanium because the high energy barrier is associated with a significant low-temperature suppression. BCC titanium is likely to be more stable because its potential energy surface is characterized by low barriers. HCP lattice is the most uncertain since a dilute hydrogen configuration is needed to obtain the correct value of diffusivity magnitude and the energy barrier.

The contributions of this study are threefold. First, a phase-resolved Arrhenius residual learning approach is used to evaluate hydrogen diffusivity in a Ti–H alloy. Second, this method is applied to three different lattices including FCC, BCC, and HCP titanium containing dilute hydrogen concentration. And finally, fused Arrhenius curves are used to evaluate the reliability of each Ti–H phase.

2 Materials and methodology

2.1 Transport values and phase classes

The analysis relies on the transport quantities specific to each phase, as given in Table 1. Three lattice structures were retained due to their corresponding different hydrogen mobilities. In FCC $Ti_{648}H_{1296}$, hydrogen diffuses in the densest titanium dihydride, with relatively low diffusivity and high apparent activation barrier. In BCC $Ti_{648}H_{648}$, the phase describes the high mobility of hydrides with low barrier. Finally, in HCP $Ti_{648}H_{36}$, a dilute hydrogen in close-packed titanium lattice was considered. Each of these lattices provides information about a distinct mobility regime that allows testing LC-ARL on an informative problem rather than a toy example. The evaluated transport values include active-learning moment tensor potential (MTP-AL), DIRECT moment tensor potential (MTP-DIRECT), and experimental references. The DIRECT approach serves as a sampling technique for interatomic potential training data in the machine-learning framework and is used in this study only as a source of transport estimates to be analyzed via the LC-ARL algorithm [1].

Table 1. Phase-specific transport values used for LC-ARL calibration. Diffusivities are provided in units of 10^{-5} cm^2 s^{-1} at the reference phase temperature T_0.

Lattice	Composition	T_0 (K)	D_{AL}	D_{DIRECT}	D_{exp}	$E_{a,\mathrm{AL}}$ (eV)	$E_{a,\mathrm{DIRECT}}$ / $E_{a,\mathrm{exp}}$ (eV)
FCC	$Ti_{648}H_{1296}$	800	0.006	0.006	0.006	0.80	0.91 / 0.92
BCC	$Ti_{648}H_{648}$	600	3.6	3.8	4.0	0.16	0.14 / 0.15
HCP	$Ti_{648}H_{36}$	1000	4.1	5.4	3.0	0.49	0.42 / 0.45

Table 1 defines the calibration problem rather than just providing input values. The FCC row demonstrates the need to consider diffusivities at a single reference temperature insufficient: MTP-AL and MTP-DIRECT provide identical reference diffusivity values but different activation barriers by 0.11 eV. At the same time, the BCC row shows the case when both values, diffusivities and activation barriers, are quite close to the experimental reference. Finally, the HCP row highlights a case when the estimate with the lower activation energy error is not the one with the smallest diffusivity error, thereby directly demonstrating whether the LC-ARL approach allows retaining diagnostic information instead of averaging it into a single value.

Figure 1 presents the structural features of the considered lattice structures, as defined in Table 1. While hydrogen content is clearly visible in the visual representations, the differences in the connectivity and the degree of hydrogen occupancy are equally important to understand the difference in residual rule application for the lattices.

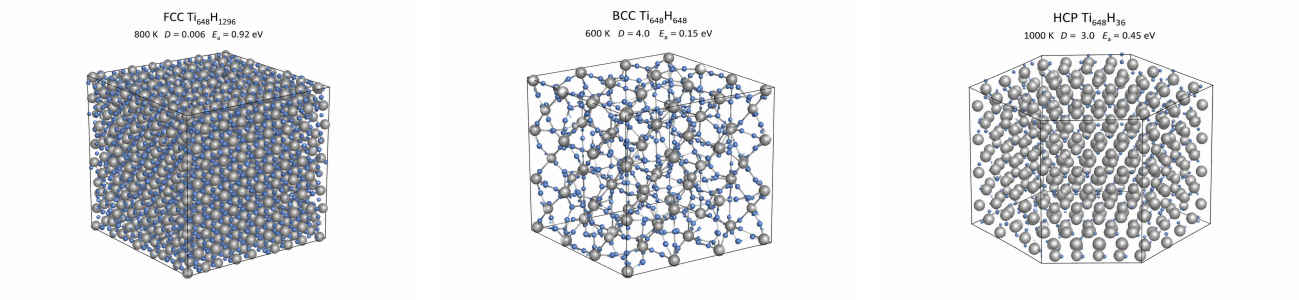

(a) FCC $Ti_{648}H_{1296}$ **(b)** BCC $Ti_{648}H_{648}$ **(c)** HCP $Ti_{648}H_{36}$

Figure 1. Phase-specific titanium–hydrogen supercell representations used to describe the LC-ARL calibration problem. FCC refers to the hydrogen-rich dihydride state at 800 K, BCC refers to the open high-mobility hydride state at 600 K, and HCP refers to dilute hydrogen in close-packed titanium at 1000 K.

The importance of Figure 1 lies in its interpretive character. While FCC can be considered as a general case of cubic solids, it represents in particular a hydrogen-rich dihydride state that may demonstrate a very high activation barrier. In turn, the BCC lattice can be interpreted as a lattice with increased openness of the structure, allowing for a high diffusion. Finally, in the case of HCP lattice, there is only a limited amount of hydrogen, making this case especially challenging for simulations. The difference in the lattices explains why phase-specific fusion rules were developed.

2.2 Arrhenius transport representation

For each lattice p and estimation method m, diffusivity is approximated using the Arrhenius equation

$$D_p^{(m)}(T) = D_{0,p}^{(m)} \exp\left(-\frac{E_{a,p}^{(m)}}{k_\mathrm{B}\,T}\right), \tag{1}$$

where $D_{0,p}^{(m)}$ is the apparent prefactor, $E_{a,p}^{(m)}$ is the activation energy, k_B is the Boltzmann constant, and T is the absolute temperature. The choice of this equation stems from its ability to separate two independent sources of hydrogen mobility. While the slope of $\log D$ is entirely controlled by the activation energy, the prefactor includes all other factors, including the number of jump attempts, available paths, and normalisation of the reference state, which is implied by the estimate. For titanium hydrides, this feature is very important since a small difference in activation energy can be negligible at the point of reference state calibration but will lead to orders-of-magnitude difference in extrapolation.

The prefactor is recovered based on the provided diffusivity at the reference temperature as

$$D_{0,p}^{(m)} = D_p^{(m)}(T_0) \exp\left(\frac{E_{a,p}^{(m)}}{k_\mathrm{B}\,T_0}\right). \tag{2}$$

This procedure ensures that each individual curve passes through the reported experimental diffusivity value and prevents accidental mixing of activation energy and diffusivity of a given lattice state. The diffusivities provided in units of 10^{-5} cm^2 s^{-1} were converted accordingly and presented in the same units.

2.3 Residual learning space

LC-ARL assigns each estimate the two-component residual vector

$$\mathbf{r}_p^{(m)} = \left[\frac{E_{a,p}^{(m)} - E_{a,p}^{\mathrm{exp}}}{\sigma_E},\ \frac{\log_{10} D_p^{(m)}(T_0) - \log_{10} D_p^{\mathrm{exp}}(T_0)}{\sigma_D}\right]. \tag{3}$$

Here, σ_E and σ_D represent the scaling constants for activation energy and logarithmic diffusivity residuals, respectively. In this study, we chose $\sigma_E = 0.05$ eV and $\sigma_D = 0.20$ decade to ensure that a moderate error of activation energy has similar importance compared to a moderate logarithmic diffusivity error. Equation (3) reflects the two independent sources of transport errors and refuses the collapse of slope and magnitude error into a single value. Namely, it first asks if the temperature dependence is correct and second if the curve is placed correctly in terms of diffusivity magnitude.

The residual loss of each estimate for phase p is defined as

$$\mathcal{L}_p^{(m)} = \left(\frac{E_{a,p}^{(m)} - E_{a,p}^{\mathrm{exp}}}{\sigma_E}\right)^2 + \left(\frac{\log_{10} D_p^{(m)}(T_0) - \log_{10} D_p^{\mathrm{exp}}(T_0)}{\sigma_D}\right)^2. \tag{4}$$

While Equation (4) can be treated as a regression target for black-box fusion method, here it serves as a tool for comparing slopes and magnitudes of experimental diffusivities and their atomistic counterparts independently of one another. Namely, squaring the normalized residuals provides an appropriate penalty for larger deviations but keeps the sign of the deviation unchanged, making the vector residual more valuable. This separation is particularly important for titanium hydrides due to different characteristics of each lattice type (FCC, BCC, and HCP).

2.4 Phase-conditioned fusion rule

In order to determine the reliability weights, a modified inverse residual formula is used:

$$w_p^{(m)} = \frac{\left[\mathcal{L}_p^{(m)} + \epsilon\right]^{-1}}{\sum_j \left[\mathcal{L}_p^{(j)} + \epsilon\right]^{-1}}, \tag{5}$$

where $\epsilon = 10^{-6}$ ensures non-zero division. Here, $w_p^{(m)}$ is inversely related to the squared norm of the residual and provides larger weight to the estimate that deviates less from experimental reference in phase-specific residual space. It should be noted that the residual is calculated separately for each phase, which is important since a better estimate in FCC lattice should not have a direct preference in HCP lattice where the residual balance is different.

The weighted average activation energy is calculated as

$$E_{a,p}^{\mathrm{LC}} = \sum_m w_p^{(m)} E_{a,p}^{(m)}, \tag{6}$$

which produces the Arrhenius slope. As can be seen, Equation (6) remains simple and interpretable as activation energy. While the weights affect final values, no additional parameters

2.5 Residual behavior of phase-specific transport values

The residual characteristics of the atomistic estimates are listed in Table 2. LC-ARL does not apply a fixed weighting scheme for the atomistic transport estimates. Instead, the weighting follows the transport behavior of each individual lattice structure. FCC titanium dihydride requires more weight for the MTP-DIRECT because the MTP-AL activation energy is 0.12 eV lower than the experimental activation energy although both estimates provide the correct diffusivity value for titanium dihydride. Because of the high activation energy of FCC, the difference in slope becomes especially important because at other temperatures than 800 K, a lower activation energy results in a lower thermal dependence and thus in an increased overlap between the diffusivity of the FCC and the other structures.

Table 2. Residual components, residual loss, and LC-ARL weights for the two potential-derived transport estimates.

Lattice	Estimate	ΔE_a (eV)	$\Delta \log_{10} D$	Residual loss	Weight
FCC	MTP-AL	-0.120	0.000	5.760	0.054
FCC	MTP-DIRECT	-0.010	0.000	0.040	0.946
BCC	MTP-AL	0.010	-0.046	0.073	0.497
BCC	MTP-DIRECT	-0.010	-0.022	0.048	0.503
HCP	MTP-AL	0.040	0.136	0.934	0.558
HCP	MTP-DIRECT	-0.030	0.255	1.403	0.442

Table 2 provides a positive answer to the first question in the present work because it demonstrates that LC-ARL creates different weighting decisions in each lattice because the residual analysis based on two transport coordinates generates conflicts. In FCC, the zero value of the diffusivity residual in both cases is misleading when it comes to assessing the suitability of a particular atomistic estimate; it was necessary to consider also the activation energy. This means that in FCC, only MTP-DIRECT can reproduce the activation-energy component. In the BCC lattice, both estimates have similar activation energy and diffusivity and thus both have approximately equal residual losses and weights. In HCP titanium hydride, there is a conflict that needs to be resolved through the weighting process. Even though MTP-AL estimates diffusivity more accurately, the MTP-DIRECT estimate predicts a much more realistic activation energy. As a consequence, both atomistic estimates need to contribute to the fusion procedure.

The least problematic case is BCC titanium hydride, which requires nearly equal LC-ARL weights. This result makes perfect sense since hydrogen migration in the open BCC structure takes place easily at a lower activation energy, and thus MTP-AL and MTP-DIRECT produce the same transport curves with nearly equal parameters. This case illustrates that in order to avoid an unphysical weighting process, it is essential to compare only those transport estimates that are not in close agreement with experimental data.

HCP titanium hydride presents the most challenging case among the investigated lattices. One can clearly see that MTP-AL provides a larger activation energy but smaller logarithmic diffusivity deviation compared to MTP-DIRECT. This is why MTP-AL gets slightly higher weight than MTP-DIRECT because of its slightly better activation energy agreement. However, this result also indicates that in dilute HCP titanium hydride, the fusion technique is capable of capturing conflicting information and thus is able to preserve it in the reconstructed transport curve. This result will help in materials development by identifying which lattice needs further testing.

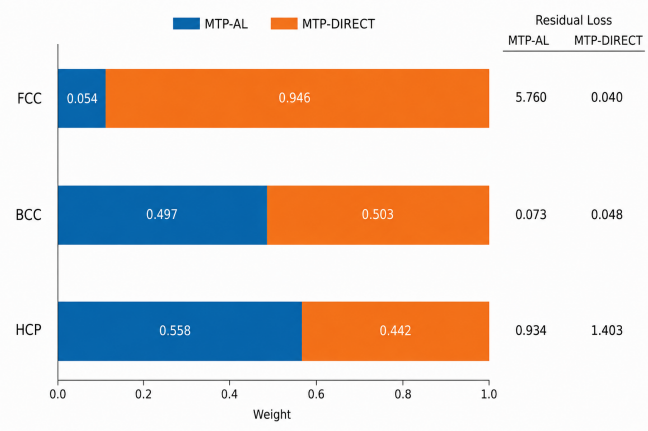

Figure 2. Phase-local LC-ARL weight allocation and residual-loss comparison for MTP-AL and MTP-DIRECT estimates. The horizontal bars show the normalized contribution of each atomistic estimate to the fused diffusivity curve, while the numerical column on the right reports the residual losses that drive the inverse-loss weighting. FCC is dominated by MTP-DIRECT due to its activation-energy agreement, BCC is equally divided between two estimates due to their proximity to the experimental reference values, and HCP is characterized by mixed weights due to conflicting transport information in the estimates.

Figure 2 helps to visualize the weighting scheme used by the proposed fusion technique. The horizontal bar for FCC indicates that one transport estimate dominates another. This happened due to the presence of significant activation-energy residual, while the diffusivity residual is practically nonexistent. In BCC titanium hydride, no dominant estimates were identified because there was no clear winner regarding the activation energy and diffusivity deviations. HCP lattice shows the most interesting behavior, where both transport estimates are given a non-negligible weight because both have a meaningful contribution to the diffusivity and activation energy. This behavior is a direct outcome of an effective two-coordinate residual scheme.

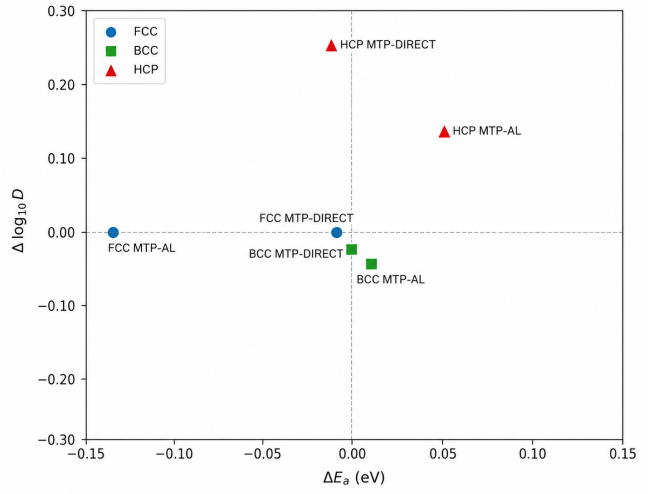

Figure 3. Two-coordinate residual map for the potential-derived transport estimates. The horizontal coordinate gives activation-energy deviation and the vertical coordinate gives logarithmic diffusivity deviation relative to the phase-specific reference values. The FCC points are separated mostly due to their activation-energy difference, the BCC points remain very close to the origin of the coordinate system, and the HCP points populate the upper-right corner with larger diffusivities and activation energies.

Figure 3 visualizes the direction of the residual components, i.e., whether the estimate matches better diffusivity (vertical coordinate) or activation energy (horizontal coordinate). Close points in the figure correspond to good transport estimates while far-apart points indicate problematic data. The horizontal displacement represents a discrepancy in activation energy, whereas vertical displacement is indicative of disagreement on diffusivity at the phase-specific reference temperature. The FCC data are mostly horizontally displaced because of the activation-energy mismatch, the BCC data are located very close to the origin because they agree well with both diffusivity and activation energy, and the HCP data are positioned in the upper-right corner because of their large diffusivity values and activation energy.

2.6 Reconstructed prefactors and fused Arrhenius quantities

The resulting transport data are shown in Table 3. Prefactor reconstruction differs for each lattice because the activation energy is always calculated according to the reference diffusivity. In FCC titanium hydride, the prefactor is relatively large because of the strong activation-energy barrier required by the high diffusion temperature of 800 K. BCC titanium hydride requires a much smaller prefactor because its activation energy is negligible, thus making diffusion at the reference temperature easy. HCP titanium sits between these two extremes in terms of its activation energy, thus the prefactor reflects its intermediate nature.

Table 3. LC-ARL fused transport quantities. Diffusivity is reported in units of 10^{-5} cm^2 s^{-1} at the phase-specific reference temperature; D_0 is expressed in cm^2 s^{-1}.

Lattice	$D_{\mathrm{LC}}(T_0)$	$E_{a,\mathrm{LC}}$ (eV)	ΔE_a (eV)	Diffusivity deviation (%)	$\log_{10} D_0$
FCC	0.006	0.904	-0.016	0.0	-1.527
BCC	3.699	0.150	-0.0001	-7.5	-3.172
HCP	4.630	0.459	0.009	54.3	-2.021

Table 3 provides a positive answer to the second research question posed in the introduction. The resulting fused parameters successfully describe phase-specific hydrogen migration behavior without blurring the distinction between the FCC and BCC phases as well as preserving the intermediate status of the HCP lattice. The average activation-energy difference for fused activation energies is 0.0084 eV, compared with 0.0567 eV for MTP-AL and 0.0167 eV for MTP-DIRECT. The reduction is achieved in all three lattices. FCC shows the largest improvement, BCC almost coincides with the experimental activation energy because of its equal weight for MTP-AL and MTP-DIRECT. HCP titanium shows slight improvement over the MTP-AL data because it combines 0.49 eV MTP-AL and 0.42 eV MTP-DIRECT.

Regarding reference diffusivity, it was successfully predicted in FCC titanium hydride since both estimates matched the experimental value exactly. The deviation of BCC diffusivity is approximately −7.5%, while HCP overpredicts the diffusivity by roughly 54%. Such results demonstrate the strength of LC-ARL for detecting problems with transport estimates as long as the data are provided correctly. For example, in dilute HCP titanium hydride, the problem of conflicting diffusivity and activation energy is detected, which shows the potential for future experimental testing of this structure.

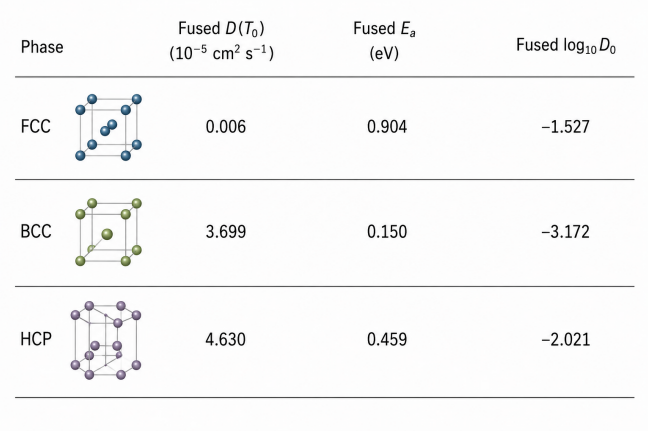

Figure 4. Phase-resolved graphical summary of the LC-ARL fused activation energies and prefactors for the three FCC, BCC, and HCP titanium hydride phases. The graph includes reference diffusivity along with the fused values, thus emphasizing the physical plausibility of slow dense FCC titanium dihydride, fast BCC titanium hydride, and the intermediate dilute HCP titanium hydride regime.

Figure 4 allows a direct interpretation of the phase-dependent transport properties. For FCC, the small reference diffusivity and large activation energy imply that this phase remains suppressed over a wide range of temperatures. For BCC, the small activation energy explains why mobility does not decrease despite falling temperature. For HCP, the uncertainty in diffusivity and activation energy implies an intermediate behavior, which is a plausible hypothesis but requires further validation. Figure 4 summarizes the numerical results by translating them into phase-resolved physics.

2.7 Temperature-dependent diffusivity and phase ordering

Figure 5a illustrates the calculated temperature dependence using the LC-ARL diffusivity curve. At each selected temperature point, the transport ordering remains as expected: BCC titanium hydride is the fastest hydrogen diffusion phase,

the intermediate hydrogen occupancy in HCP titanium leads to an intermediate temperature dependence, and FCC titanium dihydride is the slowest phase at all temperatures. The transport ordering emerges automatically from the fusion of activation energies, without imposing it artificially through some ad hoc procedure. A calibration method leading to a lower FCC barrier or a higher HCP diffusivity would disrupt the natural order of phases by overestimating their mobility.

Table 4. LC-ARL predicted diffusivity over selected temperatures. Values are reported in units of 10^{-5} cm^2 s^{-1}.

Lattice	300 K	500 K	600 K	800 K	1000 K
FCC	1.93×10^{-12}	2.30×10^{-6}	7.58×10^{-5}	6.00×10^{-3}	8.26×10^{-2}
BCC	2.04×10^{-1}	2.07	3.70	7.64	11.8
HCP	1.85×10^{-5}	2.25×10^{-2}	1.33×10^{-1}	1.22	4.63

As seen from Table 4, the inclusion of the activation-energy coordinate is crucial for preserving the known physical ordering. For example, at 300 K, the high activated barrier of FCC prevents the predicted diffusivity from recovering its reference value. Instead, BCC remains the most mobile phase at this temperature due to its low activation energy. At 800 K, FCC returns the reference value, while BCC continues to show strong mobility. HCP achieves its peak diffusivity at 1000 K but does not match BCC, although it is significantly higher. From these numbers, one concludes that BCC-like phases are critical for modeling hydrogen transport in titanium, whereas FCC acts as a slow phase with rich hydrogen distribution. HCP is relevant mainly for high temperatures and local hydrogen-rich environments.

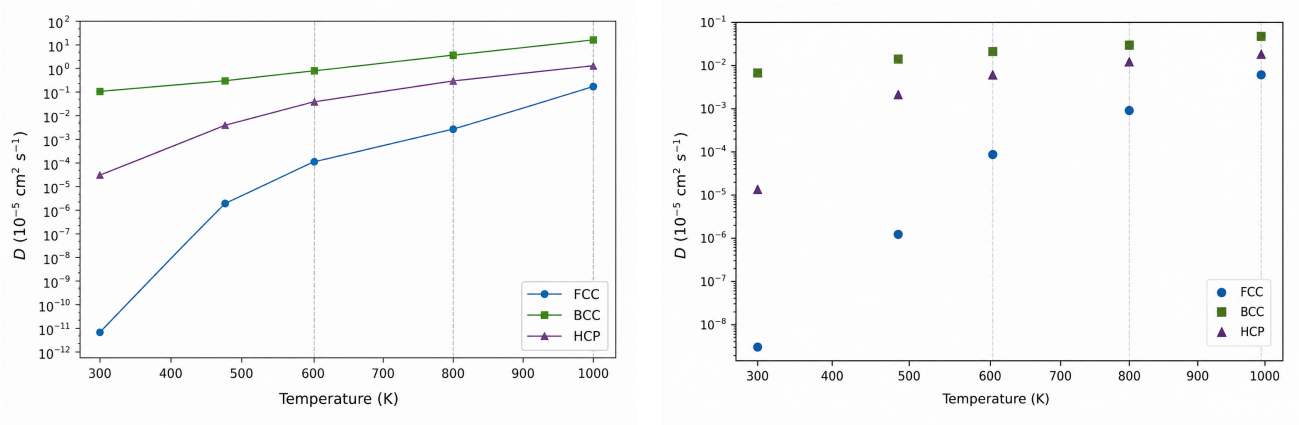

(a) Arrhenius curves **(b)** Selected temperature markers

Figure 5. Comparison of temperature-dependent diffusivities for the LC-ARL phase classes. The logarithmic axes emphasize the kinetic contrast: BCC is always the most mobile phase, HCP experiences significant rise with temperature, while FCC shows slow kinetics because of its activated barrier. Dashed vertical lines show selected temperatures for comparison of the phases.

Figure 5 directly addresses the key research question posed in the paper by visualizing the transport behavior at different temperatures. Each curve preserves the natural ordering and reflects the physical characteristics of the corresponding lattice structure. Specifically, BCC maintains the maximum diffusivity over the whole range due to its low barrier. At the same time, FCC remains suppressed due to a high barrier. Finally, HCP rises with increasing temperature, approaching the level of importance of BCC. The marker panels help differentiate between reference-temperature recovery and behavior at higher temperatures, thus demonstrating why LC-ARL considers both the activation energy and the prefactor as separate coordinates.

At 300 K, the difference between BCC and FCC diffusivities is particularly striking since the FCC activation energy is close to 0.9 eV. The exponential term in Equation 1 suppresses the curve strongly even for a relatively large prefactor. In turn, BCC shows a larger diffusivity at 300 K due to the smaller value of its activated barrier. In other words, any BCC-like lattice phase can act as a high mobility hydrogen channel, while FCC titanium dihydride represents a slow and hydrogen-rich phase.

At 800 K, FCC achieves its reference value of 6.00×10^{-3} cm^2 s^{-1}, while BCC maintains a three-orders-of-magnitude larger diffusivity. Moreover, HCP shows a significant increase in diffusivity over the temperature range, but it still stays below BCC. Finally, HCP diffusivity becomes 4.63 cm^2 s^{-1}, which corresponds to an elevated temperature level and indicates a non-negligible hydrogen distribution rate in titanium. All in all, the ordering of phases in the temperature sweep supports a phase-aware treatment of hydrogen transport in titanium, i.e., both phase fraction and local topology affect hydrogen redistribution.

The temperature sweep highlights another advantage of considering activation energy as a separate coordinate. Namely, the reference FCC diffusivities for MTP-AL and MTP-DIRECT are identical, but their activation energies differ by 0.11 eV.

At a lower temperature, this small difference produces a considerable discrepancy in predicted diffusivity. As a result, LC-ARL suppresses the contribution with the smaller activation energy, thereby preserving the strong separation between BCC, HCP, and FCC phases. In the case of BCC, the difference between activation energies is not significant enough to affect the diffusivity curve. The differences for HCP, however, become noticeable in the fused result.

2.8 Comparison with individual atomistic estimates

In order to summarize the overall performance of each of the methods, we compute the mean absolute deviation of activation energies and log diffusivities. According to Table **??**, the mean absolute activation-energy deviation is equal to 0.0567 eV for MTP-AL and 0.0167 eV for MTP-DIRECT. In turn, the mean logarithmic diffusivity deviation for MTP-AL equals 0.060 decade. For MTP-DIRECT, however, the latter quantity is larger by 0.033 decade since HCP gives an overly high diffusivity. The mean absolute deviation for activation energy and diffusivity are 0.0084 eV and 0.074 decade for LC-ARL.

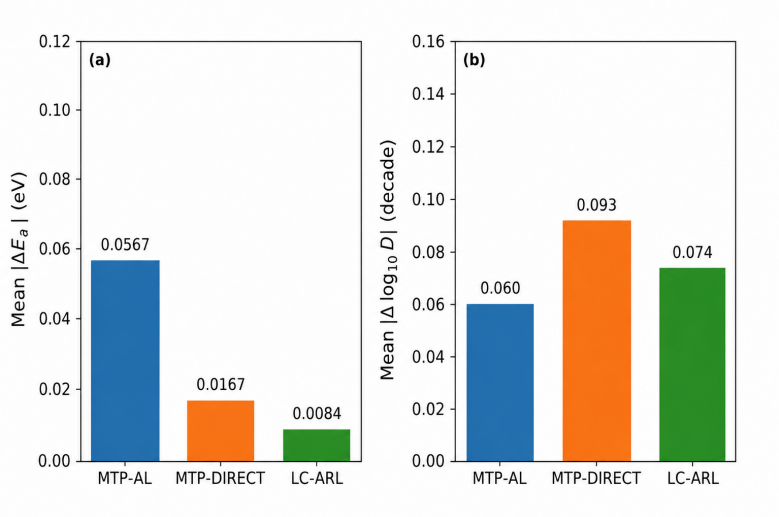

Figure 6. Aggregate comparison of MTP-AL, MTP-DIRECT, and LC-ARL in terms of activation-energy fidelity and reference diffusivity error. Panel (a) shows the mean absolute deviation of activation energies. Panel (b) displays the mean absolute logarithmic diffusivity deviation. LC-ARL provides improved activation-energy fidelity and reference diffusivity accuracy.

Figure 6 provides a quantitative comparison of the phase-resolved data, but this plot cannot substitute the latter. The mean aggregate metrics illustrate that LC-ARL has the best activation-energy fidelity and produces small errors in reference diffusivity. However, it is also essential to look at the residual maps in order to understand the reason behind the relatively poor HCP activation energy. In other words, the aggregate plot provides evidence that the fusion works well, while the residual map reveals what phase and coordinates should receive additional attention.

It is also clear from the above results that a selection of a single atomistic estimate for each phase would be counterproductive. Namely, in the case of FCC titanium, the high barrier makes MTP-DIRECT superior. For BCC, both estimates are almost equally good since they give similar activation energies and reference diffusivities. As for HCP, the larger weight for MTP-AL comes from the better reference diffusivity, while MTP-DIRECT provides a correct activation energy. Thus, LC-ARL preserves both advantages in the form of explicit weights. From a modelling standpoint, this is especially important because of the phase-specific reliability of potential generation strategies.

From a practical perspective, it is reasonable to focus on phases with higher uncertainty for validation. For FCC titanium, the need for further validation arises only if one uses the transport parameter at the boundaries of the selected temperature range, since the high barrier determines the transport behavior. BCC appears to be the most robust phase since the estimates give the correct value of activation energy and diffusivity. Finally, HCP titanium is the target phase for validation due to significant differences between the residual components of each estimate. Hence, in a future project, one may prioritize HCP simulations over BCC, although the latter phase also needs verification.

2.9 Materials interpretation and relevance to hydride technology

The results obtained in this study provide valuable insights into materials properties and modelling. Specifically, the low diffusivity of FCC titanium at lower temperatures implies that this phase acts as a hydrogen-rich reservoir. Hence, once such regions appear, their redistribution can be extremely slow if the temperature does not reach elevated levels. On the contrary, the high diffusivity of BCC implies that any BCC-like regions can play a key role in fast hydrogen redistribution.

Dilute HCP titanium, which is difficult to describe atomistically, requires further attention during modelling.

All in all, these conclusions are aligned with our knowledge about hydrogen diffusion in metallic materials [11–13]. Furthermore, these results indicate the necessity of the phase-resolved treatment during the modelling process. In practical calculations, there is always a need to derive a homogenized transport model from detailed data for atomistic simulations. However, this procedure should be performed taking into account possible fast pathways and slow hydride reservoirs, which means that phase resolution is crucial during engineering modelling.

For industry and science purposes, the use of LC-ARL is beneficial since it is lightweight. There is no need to retrain a machine learning potential or use a new surrogate model. The method only relies on the availability of reference diffusivity and activation energy for each of the phases involved. Therefore, LC-ARL can be appended to existing atomistic workflow and used for comparison of transport curves, phase prioritization, and construction of a homogenized table. Thus, the present study opens up opportunities for computational materials engineering.

2.10 Limitations and directions for future development

The present study uses one diffusivity and one activation energy for each phase. While sufficient for determining the mathematics of LC-ARL, this approach is inadequate to represent all possible transport behavior in titanium hydrides. Non-Arrhenius transport, concentration dependence of migration barrier heights, correlated experimental uncertainty, limited trajectory information, and changes in mechanisms over a wide range of temperatures require additional input. The HCP system best demonstrates the need for more information. With a small amount of mobile hydrogen in the dilute system of $Ti_{648}H_{36}$, only one reference temperature is enough to determine if the overestimation of diffusivity is due to finite sampling, local hydrogen behavior, or an intrinsic limitation with a single atomistic estimation.

A potential direction for future work involves adding multiple temperatures, concentrations, and trajectories. Additional reference points can help LC-ARL account for non-linearity or sensitivity to concentration. Using hierarchical weights may improve the differentiation between experimental uncertainty and atomistic uncertainty. An even more promising direction involves returning the LC-ARL weights to atomistic sampling. In this scenario, the residual conflict in HCP Ti-H would motivate further MD simulations at nearby concentrations of hydrogen, while the stability of the BCC case would be assumed until new information suggests otherwise. This would increase computational efficiency in discovering new materials, while maintaining interpretability of results.

3 Conclusions

The research question posed here was to determine whether a lattice-conditioned residual rule capable of separating the effects of Arrhenius-slope error and reference-diffusivity error can incorporate atomistic estimates of Ti-H diffusion into a physically coherent, phase-resolved description of diffusivity. The answer for the selected FCC, BCC, and HCP titanium hydride calibration set is yes. LC-ARL reduced the average activation-energy deviation to 0.0084 eV, improved the accuracy of Arrhenius-slopes compared to both MTP-POT estimates, and preserved the expected physical ordering of transport behavior BCC > HCP » FCC over the range of 300 - 1000 K.

The method was able to identify the controlling phase of residual variance. BCC $Ti_{648}H_{648}$ represents the most stable case due to the fact that both MTP-POT estimates agree in reproducing low-barriers and high mobilities. In contrast, FCC $Ti_{648}H_{1296}$ is mainly influenced by activation energy. Suppressing the low-barrier MTP-AL case ensures that the dihydride curve does not flatten out in an unphysical manner outside of 800 K. HCP $Ti_{648}H_{36}$ represents the most challenging situation, where there is a conflict between agreement in diffusivity magnitude and activation energy. The fusion procedure leads to overestimated fused diffusivity at 1000 K, making dilute HCP titanium the prime candidate for further trajectories, concentration, and experimental validation.

The main scientific result is not the set of recalibrated Ti-H diffusivity curves, but rather the interpretation of transport. The titanium dihydride behaves like a hydrogen-rich reservoir; the titanium hydride behaves like a rapid mobility pathway; the dilute titanium behaves as an intermediate phase with sampling and slope-magnitude errors affecting residual variance. Therefore, the paper's central research question is answered. Using phase-local representation of residuals can preserve the physics of Ti-H mobility order, while at the same time highlighting areas of minimum model confidence.

The LC-ARL method suits computational materials science thanks to its clear interpretation, reproducibility, and economy. The approach uses pre-calculated parameters, provides a physical interpretation of activation energy, and generates a list of prioritization points. To address the issue of finite trajectories, further work must focus on extending the calibration to multiple temperatures, hydrogen concentrations, and independent trajectories.

Data availability

All numerical values used in the calculations are reported in Tables 1–4. The graphical material in Figures 1–**??** visualizes the same phase classes, residual quantities, fused transport parameters, and temperature-dependent trends. The LC-ARL calculations are deterministic applications of Eqs. (1)–(**??**) to the tabulated transport values.

Conflict of interest

The authors declare no conflict of interest.

References

[1] Qi, J., Ko, T. W., Wood, B. C., Pham, T. A. & Ong, S. P. Robust training of machine learning interatomic potentials with dimensionality reduction and stratified sampling. *npj Computational Materials* **10**, 43 (2024).

[2] Leyens, C. & Peters, M. *Titanium and Titanium Alloys: Fundamentals and Applications*. Wiley-VCH, Weinheim (2003).

[3] Banerjee, D. & Williams, J. C. Perspectives on titanium science and technology. *Acta Materialia* **61**, 844–879 (2013).

[4] San-Martin, A. & Manchester, F. D. The H–Ti (hydrogen–titanium) system. *Bulletin of Alloy Phase Diagrams* **8**, 30–42 (1987).

[5] Miyoshi, T., Naito, S., Yamamoto, M., Doi, M. & Kimura, M. Diffusion of hydrogen in titanium, $Ti_{88}Al_{12}$ and Ti_3Al. *Faraday Transactions* **92**, 483–486 (1996).

[6] Sevilla, E. H. & Cotts, R. M. Hydrogen diffusion in bcc TiH_x and $Ti_{1-y}V_yH_x$. *Physical Review B* **37**, 6813–6820 (1988).

[7] Kaess, U., Majer, G., Stoll, M., Peterson, D. T. & Barnes, R. G. Hydrogen and deuterium diffusion in titanium dihydrides/dideuterides. *Journal of Alloys and Compounds* **259**, 74–82 (1997).

[8] Oriani, R. A. The diffusion and trapping of hydrogen in steel. *Acta Metallurgica* **18**, 147–157 (1970).

[9] Birnbaum, H. K. & Sofronis, P. Hydrogen-enhanced localized plasticity: A mechanism for hydrogen-related fracture. *Materials Science and Engineering A* **176**, 191–202 (1994).

[10] Robertson, I. M. et al. Hydrogen embrittlement understood. *Metallurgical and Materials Transactions B* **46**, 1085–1103 (2015).

[11] Fukai, Y. *The Metal-Hydrogen System: Basic Bulk Properties*, 2nd ed. Springer, Berlin (2005).

[12] Mehrer, H. *Diffusion in Solids: Fundamentals, Methods, Materials, Diffusion-Controlled Processes*. Springer, Berlin (2007).

[13] Wipf, H. Solubility and diffusion of hydrogen in pure metals and alloys. *Physica Scripta* **T94**, 43–51 (2001).

[14] Behler, J. & Parrinello, M. Generalized neural-network representation of high-dimensional potential-energy surfaces. *Physical Review Letters* **98**, 146401 (2007).

[15] Bartók, A. P., Payne, M. C., Kondor, R. & Csányi, G. Gaussian approximation potentials: The accuracy of quantum mechanics, without the electrons. *Physical Review Letters* **104**, 136403 (2010).

[16] Shapeev, A. V. Moment tensor potentials: A class of systematically improvable interatomic potentials. *Multiscale Modeling & Simulation* **14**, 1153–1173 (2016).

[17] Deringer, V. L., Caro, M. A. & Csányi, G. Machine learning interatomic potentials as emerging tools for materials science. *Advanced Materials* **31**, 1902765 (2019).

[18] Unke, O. T. et al. Machine learning force fields. *Chemical Reviews* **121**, 10142–10186 (2021).

[19] Chen, C. & Ong, S. P. A universal graph deep learning interatomic potential for the periodic table. *Nature Computational Science* **2**, 718–728 (2022).

[20] Zuo, Y. et al. Performance and cost assessment of machine learning interatomic potentials. *Journal of Physical Chemistry A* **124**, 731–745 (2020).

[21] Podryabinkin, E. V. & Shapeev, A. V. Active learning of linearly parametrized interatomic potentials. *Computational Materials Science* **140**, 171–180 (2017).

[22] Gubaev, K., Podryabinkin, E. V., Hart, G. L. W. & Shapeev, A. V. Accelerating high-throughput searches for new alloys with active learning of interatomic potentials. *Computational Materials Science* **156**, 148–156 (2019).

[23] Zhang, L., Lin, D.-Y., Wang, H., Car, R. & E, W. Active learning of uniformly accurate interatomic potentials for materials simulation. *Physical Review Materials* **3**, 023804 (2019).

[24] Thompson, A. P. et al. LAMMPS: A flexible simulation tool for particle-based materials modeling at the atomic, meso, and continuum scales. *Computer Physics Communications* **271**, 108171 (2022).

[25] Kresse, G. & Furthmüller, J. Efficiency of ab-initio total energy calculations for metals and semiconductors using a plane-wave basis set. *Computational Materials Science* **6**, 15–50 (1996).

[26] Kresse, G. & Furthmüller, J. Efficient iterative schemes for ab initio total-energy calculations using a plane-wave basis set. *Physical Review B* **54**, 11169–11186 (1996).

[27] Perdew, J. P., Burke, K. & Ernzerhof, M. Generalized gradient approximation made simple. *Physical Review Letters* **77**, 3865–3868 (1996).